Journal of Power Sources 418 (2019) 225–232

Contents lists available at ScienceDirect

Journal of Power Sources

journal homepage: www.elsevier.com/locate/jpowsour

Net power positive maximum power point tracking energy harvesting system for microbial fuel cell

Muhannad Alaraj[a], Jae-Do Park[b,*]

[a] Department of Electrical Engineering, Qassim University, Qassim, Saudi Arabia
[b] Department of Electrical Engineering, University of Colorado Denver, Denver, CO, 80217, USA

HIGHLIGHTS

- A net power positive energy harvesting system (EHS) for MFC is proposed.
- An MPPT algorithm is designed based on MFC reactor dynamics.
- Detailed design of harvester hardware for minimizing control power is presented.
- The proposed EHS uses only a fraction of the harvested MFC power.

ARTICLE INFO

Keywords:
Microbial fuel cell
Energy harvesting
Maximum power point tracking and controlling

ABSTRACT

Microbial fuel cells (MFCs) have been investigated as a promising renewable energy source, although harvesting energy from MFCs is not a simple task because of their low terminal voltage and output power. For an energy harvesting system (EHS) for MFC, controlling the MFC's operating point to track the maximum power point (MPP) is essential to maximize the harvested energy, but it requires a complex control system that consumes significant amount of energy. Although this control power is a critical factor because of its substantial impact on overall efficiency, it has been largely neglected. Furthermore, the transient of MFC reactor has not been taken into consideration enough for MPPT algorithms even though it could significantly affect the operation of such algorithms. In this paper, a net power positive EHS for MFC is proposed, which has a microcontroller that tracks the MPP using a novel power estimation method considering the dynamics of MFC reactor. The proposed EHS uses only a fraction of the harvested MFC power and was able to operate at a steady-state MPP without any external power. The experimental results show that the overall efficiency of the proposed system at MPP is 59.4% with a microcontroller power consumption of 8.67 μW.

1. Introduction

Most renewable energy sources, especially the low-power ones, require a very efficient energy harvesting system (EHS) considering the amount of energy they can produce. Increasing the efficiency of EHS can be achieved by minimizing the number of components and their losses. In addition, the energy harvesting algorithm of the EHS plays an important role in the efficiency of the system and it needs to be carefully designed to reduce the power consumption. Practically, building a net power positive EHS is critical to make the system self-sustainable.

Microbial fuel cell (MFC) is a renewable energy source that the bacteria inside the reactor generate electricity while consuming organic matter. The amount of power from an MFC depends on the operating point and there is a specific one, maximum power point (MPP), where the maximum power can be extracted [1]. The MPP can be changed during operation due to various reactor conditions; hence, it needs to be tracked to keep extracting the maximum available power for the given reactor conditions. Numerous MPP tracking (MPPT) algorithms have been proposed; however, the power consumed by the control circuits has been largely neglected in the previous investigations. For example, a personal computer [2–4] and powerful microcontrollers [5,6] were used to do the required calculations, but the power used for control circuitry was not included in the overall efficiency calculation. It is not practical because the control power is non-negligible compared to the available power from an MFC. Furthermore, the MFC reactor dynamics needs to be considered for an MPPT algorithm because they move the operating point from one point to another in order to track MPP, which is substantially affected by the reactor transient.

* Corresponding author.
E-mail address: jaedo.park@ucdenver.edu (J.-D. Park).

https://doi.org/10.1016/j.jpowsour.2019.02.042
Received 16 October 2018; Received in revised form 8 February 2019; Accepted 11 February 2019
Available online 23 February 2019
0378-7753/

Designing a self-powered EHS for MFC is a challenge because typical MFC power is so low that using some of it to energize the EHS would significantly reduce the overall efficiency, even down to an impractical level. Various self-powered EHS for MFCs have been reported [7–10]; typically, they share the idea of charging a supercapacitor to a certain voltage level either directly or using a charge pump before a dc-dc converter is enabled to boost the voltage. The major disadvantage of this approach is that there is no control over the operating point of MFC. Sustained operation at MPP is not possible, which results in harvesting less power than the MFC can actually supply. Self-powered EHSs operating at MPP were reported in Ref. [11], but the method to find the MPP has an issue for some reactors that have long time constant for voltage recovery, because it uses direct open-circuit voltage (OCV) sampling, which can result in operating far from the MPP unless the circuit is opened for long period of time. An idea of minimizing the energy consumption of the control circuit was discussed in Ref. [12] by increasing sampling time and spending more time in *sleep mode* when using low power microcontrollers. However, the algorithm was tested using a personal computer and the power consumption of actual low power microcontrollers was not extensively investigated.

In this paper, a self-powered EHS with an efficient MPPT algorithm considering the transient behavior of MFC reactor is proposed. The proposed MPPT algorithm uses the MFC electrical characteristics to estimate the output power by only measuring voltages, which saves power consumption for current measurements. The proposed EHS is implemented in an ultra-low power microcontroller that uses MFC power only.

2. Methods and materials

2.1. Microbial fuel cell

2.1.1. Equivalent circuit

Electricity generation in MFCs is achieved using anaerobic bacteria such as Geobacter and Shewanella, where they consume organic matter inside the anode chamber of an MFC reactor and generate extracellular electrons that are transferred to the cathode electrode. When an external load is connected between the anode and cathode electrodes, it results in delivering electrical power to the load [1,13,14]. MFC's power generation capability has been substantially improved during the last decade, and they have been investigated as a power source for various applications including underwater remote wireless sensors [15–17]. A conceptual diagram of MFC is shown in Fig. 1a.

The MFC equivalent circuit [18] used in this paper is shown in Fig. 1b. This equivalent circuit models the MFC voltage dynamics with internal resistances and a shunt capacitor. This dynamic behavior of MFC voltage is important in tracking MPP to determine a correct steady-state power. The internal voltage V_{int} of the equivalent circuit, which is also known as OCV, can be found by opening the terminals of MFC for long enough time. To find the value of R_2, a load needs to be connected to the MFC and the terminal voltage V_T^- and output current I^- are measured. Then, the circuit is opened and terminal voltage V_T^+ is measured. The $(-)$ and $(+)$ superscript denotes the measurement right before and after the circuit opening, respectively. It is assumed that the capacitance is high enough so that the output terminal voltage is reasonably close to the capacitor voltage V_C right after opening the circuit. The resistance R_2 can be calculated as

$$R_2 = \frac{V_C - V_T^-}{I^-} = \frac{V_T^+ - V_T^-}{I^-}. \tag{1}$$

The value of the resistance R_1 can be calculated by subtracting R_2 from the total internal resistance, which can be found from the polarization curve considering that the external resistance is equal to the internal resistance at the MFC MPP. The total internal resistance can be calculated using

$$R_{int} = \frac{V_{MPP}}{I_{MPP}}, \tag{2}$$

where V_{MPP} and I_{MPP} are the voltage and current at the MPP, respectively. Then, R_1 can be given as

$$R_1 = R_{int} - R_2. \tag{3}$$

2.1.2. Transient dynamics

Using the values of V_{int}, R_1, and R_2, the shunt capacitance can be found along with the open circuit test results. From an initial capacitor voltage $V_C(0)$ when a load was connected to the terminals of MFC, the capacitor voltage will start increasing when the circuit is opened. The dynamics of the capacitor voltage can be described as follows (Detailed derivation of the capacitor voltage dynamics can be found in the supplement material).

$$V_C(t) = V_{int} + V_C(0)e^{-\left(\frac{1}{CR_1}\right)t} - V_{int}e^{-\left(\frac{1}{CR_1}\right)t} \tag{4}$$

A load should be connected to the terminals of MFC to have the current flowing before the open circuit test. Once the circuit is opened, V_C is measured two times; the initial capacitor voltage $V_C(0)$ and the voltage after t seconds $V_C(t)$. Those measurements can be used in (4) to find the capacitance C. The results of the reactor tests and identified parameters are shown in Table 1.

The internal capacitor voltage V_C in steady-state, assuming constant terminal voltage V_T , can be found as

$$V_C = V_{int} - IR_1, \tag{5}$$

where I is the current that is flowing through R_1 and R_2. Hence, the capacitor voltage can be given as

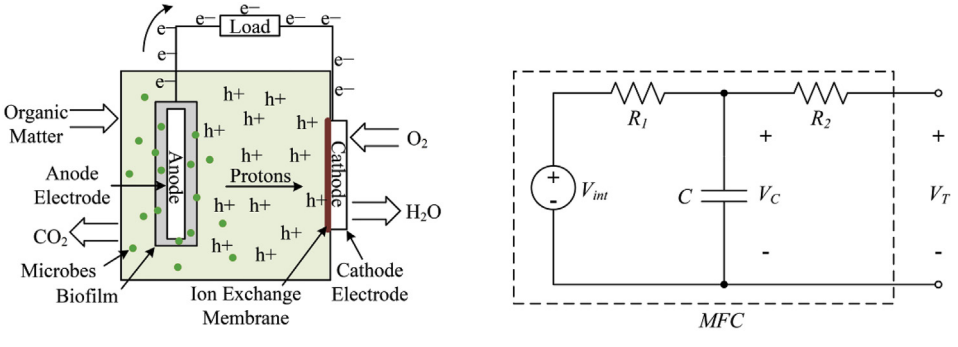

Fig. 1. (a) MFC conceptual diagram. (b) MFC electrical equivalent circuit [18]: V_{int} is MFC internal voltage, V_T is MFC terminal voltage, and R_1, R_2, and C, represents input series resistance, output series resistances, and equivalent double-layer capacitance, respectively.

Table 1
Results of MFC tests and identified equivalent circuit parameters.

Polarization curve results			Short circuit test results			Open circuit test results			Equivalent circuit parameters			
V_{OCV}	V_{MPP}	I_{MPP}	V_T^-	V_C	I	$V_C(0^-)$	$V_C(t)$	Δt	R_{int}	R_2	R_1	C
425mV	212mV	0.554mA	176mV	208mV	0.38mA	331mV	411mV	40s	378.65Ω	84.21Ω	294.44Ω	71.4mF

$$V_C = V_{int} - \frac{V_{int} - V_T}{R_1 + R_2} R_1. \tag{6}$$

The internal capacitor voltage is proportional to the terminal voltage, assuming constant equivalent circuit parameters. The time-domain dynamics of capacitor voltage with a load can be found as

$$V_C(t) = \underbrace{\frac{V_{int} R_2 + V_{T_0} R_1}{R_1 + R_2}}_{\text{Steady state value}} - \underbrace{\frac{\Delta V R_1}{R_1 + R_2}}_{\text{Decays to zero as } t \to \infty} e^{-\left(\frac{R_1+R_2}{CR_1R_2}\right)t}. \tag{7}$$

Note that the first term is the steady-state value in (6) and the second term exponentially decays to zero.

The transient behavior of MFC in (7) clearly shows that the MFC terminal voltage takes time before it reaches a steady-state value when moving from one operating point to another. Measuring the MFC power before the voltage reaches the steady-state value results in a transient value, which is either higher or lower than the steady-state power. When the MFC terminal voltage is reduced by the MPPT algorithm, the capacitor voltage will decrease to the new steady-state value, as shown in (6). The MFC current will be higher than the steady-state current because the energy stored in the capacitor is discharged during the transient. This continues until the capacitor voltage reaches the steady state. On the other hand, when the MFC terminal voltage is increased, the current is lower during this transient, because some of MFC current is charging the internal capacitor.

Therefore, the sampling time T_s should be large enough for the capacitor voltage to reach a steady-state value, because measuring MFC current before the capacitor voltage reaches a steady state will result in an erroneous power reading. The minimum sampling time for the capacitor voltage can be extracted from (7). The time constant of the capacitor transient equation is

$$\tau = \frac{CR_1R_2}{R_1 + R_2}. \tag{8}$$

The sampling time T_s needs to be

$$T_s > 5\tau \tag{9}$$

in order for 99% of the steady-state value to be measured. For the MFC reactor used in this work, the minimum sampling time is calculated as 23.31s based on the equivalent circuit parameters. Fig. 2 shows the calculated capacitor voltage using (7), when the terminal voltage was increased from 220 mV to 240 mV. Note that the initial and steady-state capacitor voltages are higher because of the R_2 drop by load current. It can be seen that the capacitor voltage reaches the steady state after around 23s.

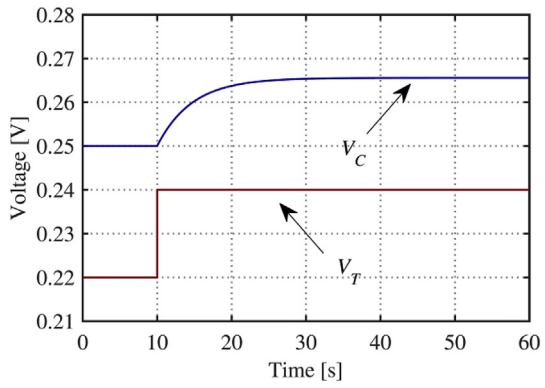

Fig. 2. The calculated capacitor voltage when the terminal voltage was increased from 220 mV to 240 mV based on the equivalent circuit model.

Generally, MPPT algorithms require the calculation of output power for each operating point from MFC voltage and current. Measuring MFC voltage is straightforward since microcontrollers can directly measure voltages, while current measurement is not. Typically, a shunt resistor is used to measure the voltage across it. Although a small shunt resistance would be better for low power loss and voltage drop, an amplifier might be needed to measure the low shunt voltage, which can consume relatively high power compared to MFC's output power. In Ref. [6], an instrumental amplifier (INA122, Texas Instruments, TX) was used, which takes non-trivial 60 μA operating at 2.2 V [19] while the MFC generating about 400 μW. Hence, an MFC output current estimation method using the characteristics of MFC is developed in this paper to reduce the power consumption of the control circuit.

2.1.3. MFC reactor

A single-chamber air-cathode MFC reactor was used in the experiments of this paper. The 60 mL anode chamber was built using a custom-built (5 cm × 5 cm x 3.5 cm, 4.5 cm internal cylinder diameter) and commercial off-the-shelf plastic blocks (5 cm × 5 cm x 2 cm, 3 cm internal cylinder diameter, Physichemi, Hong Kong). A 2.75 cm diameter and 4 cm long carbon brush (Zoltek PX35 Carbon Fiber) on a titanium rod (Millrose, OH) was used as anode electrode. The cathode electrode is made of a circular carbon paper (30 mm diameter) that contains 0.5 mg/cm2 of Pt (10% of Pt/C catalyst, 30% wet proofing). The current collector in cathode electrode is made of a small piece of 1-mm titanium wire (45485-BY, Alfa Aesar, MA) that touches the carbon paper. Four 10–24 stainless steel bolts and nuts were used to hold the blocks and electrodes together. The reactor solution leakage was avoided by installing rubber gaskets between blocks.

The reactor was inoculated using a sludge collected from a local waste water treatment plant, with a sodium acetate (2 g/L CH3COONa) and some vitamins in a 50 mM phosphate buffer solution (PBS, CH3COONa, 0.31 g/L NH_4Cl, 0.13 g/L KCl, 3.321 g/L $NaH_2PO_4.2H2O$, and 10.317 g/L $Na_2HPO_4.12H_2O$). The inoculation was repeated until the reactor terminal voltage reached 350 mV with 1 kΩ load. Then, the reactor was maintained with a 2 g/L sodium acetate in the PBS.

The procedure to refresh the medium is simple; the PBS is prepared and the sodium acetate is added to the PBS with a concentration of 2 g/L. Then the old medium inside the reactor is drained and the reactor is filled with the new medium. We waited until the voltage of the reactor goes down below 50 mV before the medium is replaced. The time between replenishments depends on the reactor size and other reactor conditions; for the reactor under test, the voltage goes down to that low level in 2–3 days.

2.2. Proposed method

2.2.1. Current estimation

In this paper, an estimated current is used in order to improve the overall efficiency of the control circuit because measuring the actual current requires additional components and power. From the equivalent circuit model in Fig. 1b, the load current is given as

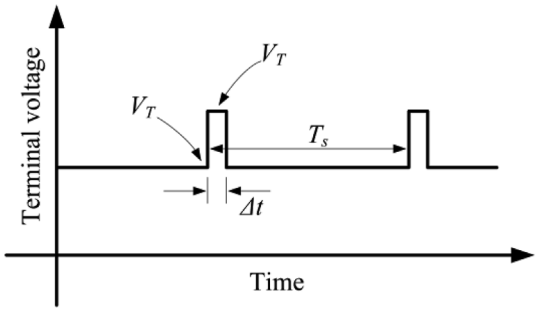

Fig. 3. Graphical representation of V_T and V_C measurement process: V_T is measured just before opening the circuit, V_C is measured right after the circuit is opened, Δt time required to measure V_C, and T_s is the sampling time.

$$I_{MFC} = \frac{V_C - V_T}{R_2} \tag{10}$$

and the current can be estimated with V_T and V_C from the open circuit test assuming that R_2 is constant, which is a reasonable assumption [18]. A graphical representation that shows the process of measuring V_T and V_C is shown in Fig. 3. It can be seen that the terminal voltage increases instantaneously as much as the voltage drop across R_2.

This method for current estimation improves the overall efficiency because it does not require any additional component for current measurement. Although the MFC energy will not be harvested during the open circuit period Δt, the energy loss is practically negligible because the opening duration is very short (around 15 ms in this work) compared to the sampling time T_s (30s), which is the harvesting period.

2.2.2. Power calculation and MPPT

Based on the calculated current (10), the MFC power can be obtained by

$$P_{est} = \frac{V_C - V_T}{R_2} V_T \tag{11}$$

However, the perturb and observe (P&O) algorithm [2,3,20] that is used in this paper to track MPP does not require the actual value of power for the operation of the algorithm as long as the relative amount of the power of two consecutive operating points is known. Therefore, the value of R_2 can be removed from (11), which results in a proportional estimated power

$$\tilde{P}_{est} = (V_C - V_T)V_T \tag{12}$$

The algorithm will converge to MPP even if R_2 changes, assuming that it does not change between two samples, which is a reasonable assumption [18].

2.2.3. Proposed algorithm

It has been shown that it takes time for an MFC to change operating points because of the high internal capacitance. This time period should be considered when tracking MPP because measuring MFC current before the capacitor voltage reaches steady-state will affect the power calculation and mislead the MPPT algorithm. A flow chart that describes the operation of the proposed algorithm is shown in Fig. 4.

The proposed MPPT algorithm in this paper is based on the P&O algorithm, but it takes the transient of the MFC voltage into consideration. It measures V_T and V_C at one operating point and calculates the proportional estimated power (12) based on the equivalent circuit model. Then the operating point is changed, and after a sampling time T_s, V_T and V_C of the new operating point are measured, as shown in Fig. 3, to calculate the new proportional estimated power. By comparing the powers of the two operating points, the system moves to the direction that gives higher power.

The contribution of the proposed algorithm on conventional P&O algorithm is the detection of power change based on the model-based current estimation and the derivation of minimum sampling time T_s that guarantees the measurement of the steady-state MFC power.

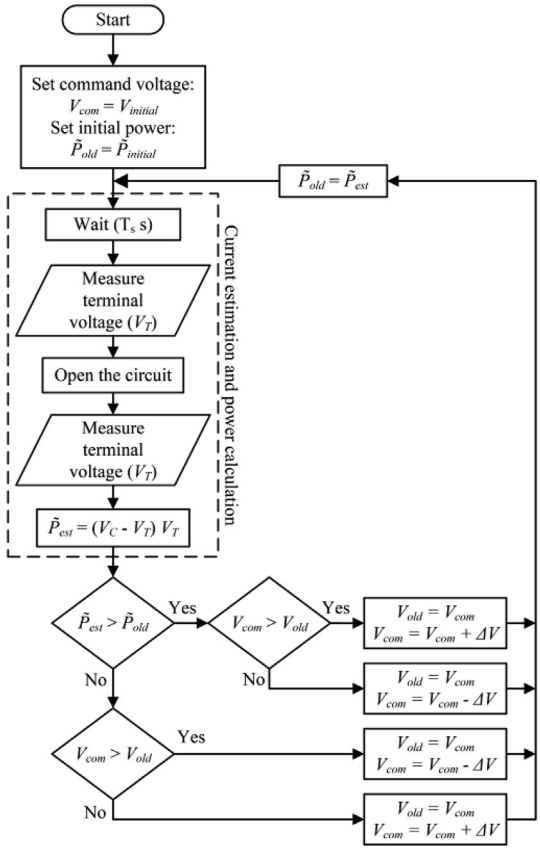

Fig. 4. Flow chart of the proposed MPPT algorithm.

2.3. System implementation

In the proposed EHS, the MFC power is handled using a commercial off-the-shelf boost converter (BQ25504, Texas Instruments, TX), which is efficient and capable of operating from MFCs' low output voltage. An ultra-low power consuming microcontroller (MSP430L092, Texas Instruments, TX) is used to control the boost converter with the proposed MPPT algorithm. The overall schematic diagram of the proposed EHS is shown in Fig. 5.

2.3.1. Boost converter

The BQ25504 is designed to operate at input voltages as low as 100 mV that covers typical MFC output voltage range. The boost converter has a built-in MPPT function that finds the OCV and sets the operating point to half of the OCV. However, the OCV is measured after opening the circuit for just 256 ms, which is substantially short for an MFC to reach its OCV. It has been shown that applying this built-in MPPT function to an MFC results in an operating point far from the MPP of the reactor [12]. The MPPT performance can be improved by using the proposed algorithm with this built-in function disabled. The input voltage of BQ25504 (i.e., MFC output voltage) can be maintained by its hysteresis controller at a reference voltage V_{ref}, which is fed by the proposed MPPT algorithm and microcontroller.

Since the proposed MPPT algorithm opens the circuit in order to measure the internal shunt capacitor voltage, a high side load switch (TPS22860, Texas Instruments, TX) is used at the boost converter's input and controlled by a microcontroller's general purpose input/output (GPIO). The switch is only opened at the time of V_C measurement, otherwise it is closed. This load switch has a very low on-

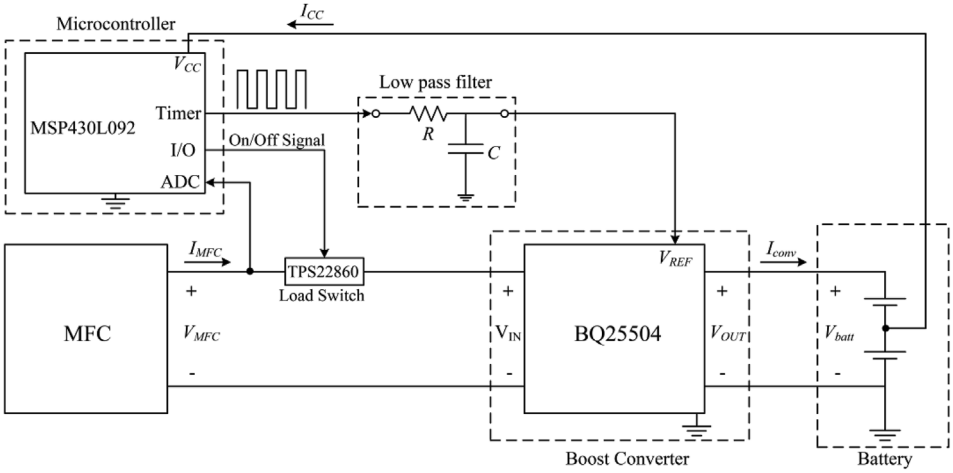

Fig. 5. Schematic diagram of the overall EHS system.

resistance; hence it does not significantly affect the overall efficiency.

As a minimum output voltage of 1.8 V is required for BQ25504 to operate, two rechargeable batteries (Ultra Last Ni-Mh, 1.25 V) connected in series are used at the output of the boost converter to store the harvested energy and maintain the output voltage at nominal 2.5 V.

2.3.2. Microcontroller and control power consumption

The designed control system uses an MSP430L092 to monitor the operating point of the MFC and control the power circuit in the EHS. The microcontroller is selected because of its low power consumption and operating voltage. It also has a built-in analog-to-digital converter (ADC) and timer/capture for pulse width modulation (PWM) and sampling time control. The anode of MFC is connected to the microcontroller's ADC to measure V_T and V_C, and a low pass filter is connected to a timer channel to generate V_{ref} for the boost converter.

The main power consumer in the control circuit is the microcontroller. Its power consumption can be reduced by staying in the *sleep mode* most of the time and switching to the *active mode* only when it is needed. According to our lab experiments, MSP430L092 consumes up to 78 μA in *active mode* when operating at 1.65 V and 1 MHz compared to only 8 μA in *sleep mode*. The time between two power measurements affects the power consumption of the microcontroller because measurements should be done in active mode. Higher sampling time means lower energy consumption because the microcontroller consumes more power in active mode, which can be shown using the microcontroller power calculation using an average current.

$$I_{ave} = \frac{1}{T_s}\left(\int_0^{T_s-\Delta t} I_{sleep}\,dt + \int_{T_s-\Delta t}^{T_s} I_{active}\,dt \right), \tag{14}$$

$$P_{ave} = V_{CC} I_{ave}, \tag{15}$$

where I_{ave} and P_{ave} are the average microcontroller current and power consumption, I_{sleep} and I_{active} are the microcontroller current at *sleep mode* and *active mode*, T_s is the sampling time, and Δt is the *active mode* time. A trade-off between energy consumption and operation performance needs to be made because frequent sampling yields faster convergence; however, the sampling time should satisfy the requirement in (9). In this paper, a sampling time T_s of 30s was used.

The energy consumption of MSP430L092 depends on its clock frequency, where it consumes up to 101 μA when operating at 1.65 V and 1 MHz compared to only 42 μA at 125 kHz [21]. Operating with such high frequencies (1 MHz and 125 kHz) requires the high frequency oscillator (HFO) that consumes up to 22 μA [21]. In MSP430L092's sleep mode, the HFO is turned off and the low frequency oscillator (LFO, typically 20 kHz) that only consumes 0.6 μA is used. Although the high frequency clock is needed for fast microcontroller performance in the *active mode*, LFO is used in both modes of operation to minimize power consumption in this paper.

The supply voltage VCC is another factor of microcontroller energy consumption. The MSP430L092 operates in a range of supply voltages (0.9–2.2 V). Higher supply voltage increases the power intake and reduces the overall efficiency of the EHS. The advantage of using higher VCC is that HFO and LFO can generate higher clock frequencies to enhance the performance, but lower supply voltage reduces the power consumption of microcontroller. However, the MSP430L092 requires a minimum supply voltage of about 1.25 V to be started, and once started it can operate with as low as 0.9 V [21]. Therefore, the bottom battery at the boost converter output is used to supply the microcontroller, which has a nominal voltage of 1.25 V and that is high enough for the microcontroller to operate. Although the batteries in this work should be initially charged to start operation, the stored energy will not be used once the system starts operating because the system is self-sustainable. Furthermore, a separate self-startup circuit can readily be used in conjunction with the proposed system.

Another power consumer in the microcontroller is the built-in analog pool for digital-to-analog converter (DAC) and ADC. Our lab experiments suggested that the microcontroller consumes 35 μA at 1.3 V when the analog pool is configured as ADC and turned on continuously and an analog-to-digital conversion takes up to 5 μA additionally. On the other hand, the microcontroller only consumes about 5.5 μA when the analog pool was turned off. Therefore, the analog pool usage needs to be minimized in order to reduce the microcontroller's power consumption. Considering that the sampling time is 30s in this work, having the analog pool turned on only at the time of measurement substantially reduces the energy consumption because the microcontroller only needs 15 ms for the required measurements. Using the actual values in (14), the average current results in 5.517 μA, which is very close to the current when the microcontroller was sleep and the analog pool was turned off all the time.

2.3.3. EHS operation to control MFC

The proposed system measures MFC terminal voltage using the microcontroller's ADC and the MFC power is calculated using the proposed method in 2.2.2; the proposed MPPT algorithm calculates the desired MFC voltage based on it. Then, the microcontroller generates a command voltage V_{ref} for the boost converter, and the boost converter controls the MFC voltage to be equal to V_{ref}, which moves the operating point closer to MPP of the reactor. Then, that cycle is execute again and the MFC power is calculated and a new desired V_{ref} is calculated, which is fed again to the boost converter to move the operation toward MPP.

Generating V_{ref} using DAC is inefficient because it requires the analog pool turned on all the time. Therefore, a low-pass filtered PWM

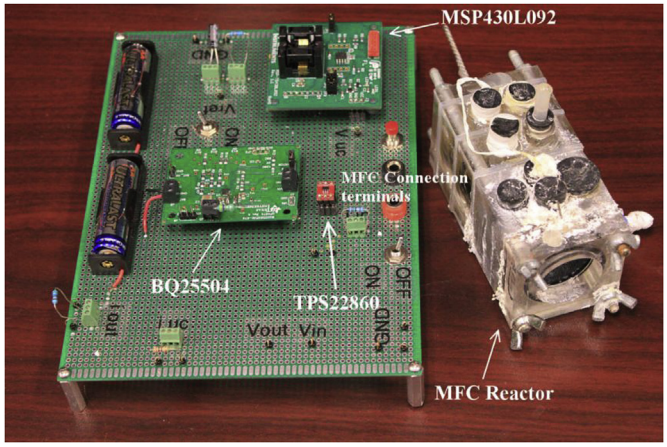

Fig. 6. Experiment set up picture: the MFC reactor and the used circuit.

is used. The timer generates a PWM signal based on its input clock signal, and since the timer can get the LFO clock signal during both *active* and *sleep mode*, it can generate the PWM signal continuously. The PWM generation in our lab experiments did not show a significant impact on the microcontroller's power consumption. The value of the DC component in the PWM signal depends on the duty cycle D and V_{CC} of the microcontroller.

$$V_{ref} = DV_{CC} \tag{16}$$

The experiment setup, the proposed EHS and MFC reactor used, is shown in Fig. 6.

3. Experimental results

The MFC voltage and current were monitored using two digital multimeters (390A, B&K Precision) during the experiments. Having a sampling time of 30s makes it easy to manually record the measurements for each operating point.

3.1. MPPT

The output voltage V_{MFC} and current I_{MFC} waveforms as well as the reference voltage for power converter V_{REF} are shown in Fig. 7a. The reactor's OCV and MPP is approx. 225 mV and 112 mV, respectively, at the time of measurement. It can be seen that the reactor generates about 65 μW at its MPP. It should be noted that the reactor was in a different batch cycle and hence it does not match with the polarization curves in Fig. 7b. The reactor under test showed MPP in the range of 65–119.11 μW at 163–255.1 mV in 4 batch cycles with an average of 100.67 μW and variance of 432.72 μW^2. Note that the variance is large because each MPP was measured at different time during each batch cycle.

The result of the proposed MPPT algorithm is shown in Fig. 7b. The straight lines represent the current voltage (I-V) relationship (i.e., polarization curve), which were plotted based on the measurements of the voltage and current during the MPPT operation. The current-power curves were also calculated based on I-V curves and plotted. The circles represent the operating points of the MFC commanded by the MPPT algorithm and the lines between the circles show the direction of transitions. Note that the algorithm stays 30s in each operating point due to the sampling time. It can be clearly seen that the MPPT algorithm was able to reach and maintain the operation around MPP starting from an initial voltage of 379 mV. It is also shown that the algorithm was able to track the varying MPP. This validates the performance of the proposed real-time MPPT algorithm.

The oscillation around MPP is about 40 mV (≈10% from MPP voltage) as can be seen in Fig. 7b, which is because of using large perturbation steps due to the low resolution of the analog-to digital converter (ADC) in the used ultra-low power microcontroller. Large steps help the microcontroller to differentiate between two operating point voltage levels; however, using powerful microcontrollers can easily increase the measurement accuracy if necessary. Although operating in smaller steps and reduce the oscillations, it will definitely consume more power. Oftentimes it is more than MFC can generate.

3.2. Efficiency

The efficiency of the system was calculated by measuring the boost converter input and output power as well as the microcontroller's power consumption and load switch power loss. The measurements and the power calculations at MPP for the efficiency calculation are shown in Table 2. The equations for calculating the input power, output power, microcontroller power, boost converter efficiency and overall EHS efficiency are included in the supplementary material.

It should be noted that the currents were measured using shunt resistors and the power across those shunt resistors was not included for the overall efficiency calculation since those resistors are only needed

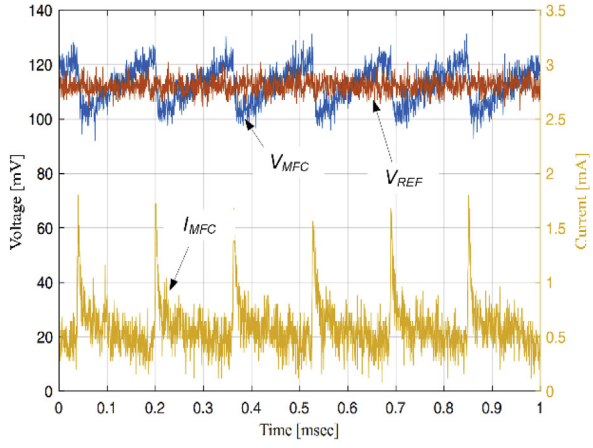

(a)

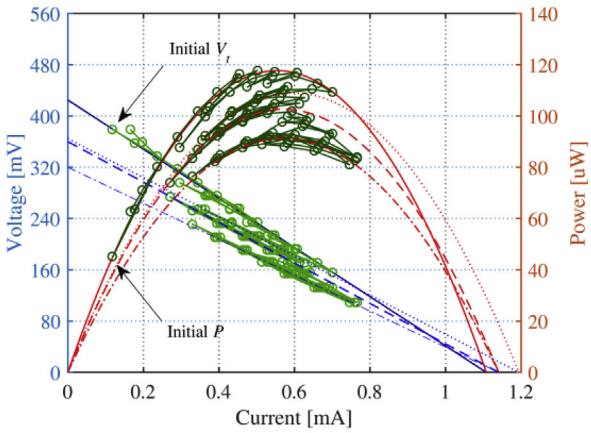

(b)

Fig. 7. Experiments: (a) MFC output voltage, output current, and reference voltage for BQ25504. MFC's OCV and MPP is approx. 225 mV and 112 mV, respectively, at the time of measurement. (b) MPPT results. Circles represent the operating points of the MFC.

Table 2
Results of voltage and current measurements and power calculations.

MFC generated power			Load switch loss			Converter output			Controller loss		
V_{MFC}	I_{MFC}	P_{in}	I	R_{ON}	$P_{LS_{loss}}$	V_{batt}	I_{conv}	P_{out}	V_{CC}	I_{CC}	$P_{\mu C}$
$213mV$	$0.5592mA$	$119.11\mu W$	$0.5529mA$	0.63Ω	$0.2\mu W$	$2.62V$	$30.3\mu A$	$79.39\mu W$	$1.3V$	$6.67\mu A$	$8.67\mu W$

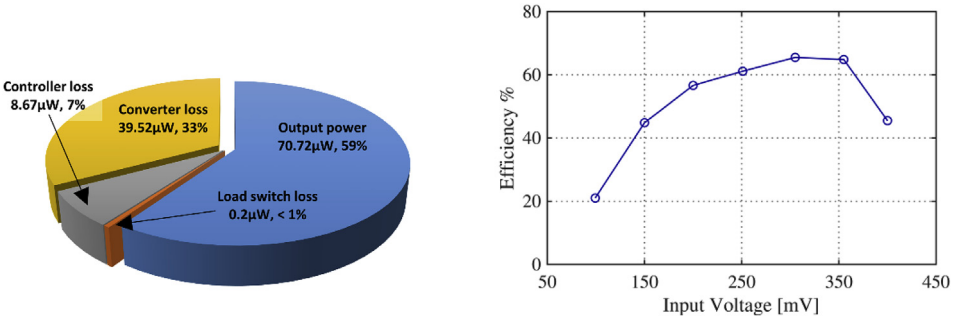

Fig. 8. Experiments: (a) The efficiency of the proposed system with different MFC operating points. (b) Power expenditure pie chart including output power, converter loss, controller loss, and load switch loss.

for efficiency calculation and not used for the system control. For the input shunt resistor, the loss was subtracted from the input power, and for the two output current shunt resistors, their power loss was added to the output power.

The boost converter efficiency was calculated at MPP to be 66.7% using (19) in the supplementary material and since the microcontroller takes about 8.67 μW, the EHS overall efficiency was calculated to be 59.4% using (20) in the supplementary material.

A pie chart for the power expenditure of each system component and the overall efficiency of the proposed EHS at different MFC operating points are shown in Figs. 8a and 8b, respectively. It can be seen that the efficiency is better with higher input voltages (> 60% in 250–350 V range); however, the MFC current decreases as well as the MFC power when the MFC voltage becomes closer to the OCV. Hence the efficiency starts to decrease at higher voltage operating points (> 350 mV).

4. Discussion

Table 3 shows a summary of this work and a comparison with other existing MFC EHSs. Existing self-sustainable systems typically do not have complete MPPT capability with self-sustainability and fall into one of the following categories: i) self-sustainable but no control over operating point, ii) MPPT capable but not counting control power usage, or iii) self-sustainable, MPPT-capable, but needs to open terminals and wait long time to measure OCV. This paper provides a highly efficient net power positive MFC EHS that can accurately track MPP considering slow MFC voltage dynamics and it requires to disconnect the MFC for only a very short time.

The proposed system needs initial voltage at the output of the boost converter to close the load switch and start harvesting. Although the system has to be self-bootable to be completely stand alone, the self-startup feature has not been included in this work due to the limitation of commercial off-the-shelf parts. However, low voltage startup circuits, e.g., < 100 mV with CMOS devices, have recently been investigated and reported in the literature. Authors' group is also working on a separate startup circuit to integrate with the harvesting part of the EHS.

5. Conclusion

In this paper, an efficient self-sustainable EHS was proposed. The system tracks MFC MPP using P&O algorithm based on the novel model-based current estimation method. The optimal power sampling time was derived for precise steady-state power measurement. Using that current estimation method and the sampling time, the proposed MPPT algorithm was able to efficiently estimate the steady-state MFC power and successfully tracked the varying MFC MPP. A commercial off-the-shelf microcontroller was configured to consume only 8.67 μW to implement the proposed MPPT algorithm and power converter control. The proposed EHS demonstrated net power positive energy harvesting from a 119 μW MFC reactor with 59.4% overall efficiency at MPP.

Acknowledgements

This work was supported by the National Science Foundation under

Table 3
Performance summary and comparison of the existing EHS.

Specification	[7]	[10]	[11]	[22]	[23]	[24]	This paper
Self-sustainable	Yes	Yes	Yes	Yes	Yes	Yes	Yes
MPPT	No	No	Yes	No	No	No	Yes
Converter	L6920DB	Custom	Custom	Custom	Custom	Custom	BQ25504
Input voltage	NA	≥300 mV	300–720 mV	≥300 mV	≥600 mV	350–480 mV	≥100 mV
Input source	MFC	MFC or PV	MFC	MFC	Miniaturized MFC	PV or TEG	MFC
Output voltage	3.3 V	3 V	2.5 V	3.3 V	0.9–1.2 V	1.4 V	2.5 V
Efficiency	NA	55%	58%	35.03%	85%	65%	59.4%

Award 1511568.

Appendix A. Supplementary data

Supplementary data to this article can be found online at https://doi.org/10.1016/j.jpowsour.2019.02.042.

References

[1] B.E. Logan, B. Hamelers, R. Rozendal, U. Schroder, J. Keller, S. Freguia, P. Aelterman, W. Verstraete, K. Rabaey, Microbial fuel cells: methodology and technology, Environ. Sci. Technol. 40 (2006) 5181–5192, https://doi.org/10.1021/es0605016.

[2] R.P. Pinto, B. Srinivasan, S.R. Uiot, B. Tartakovsky, The effect of real-time external resistance optimization on microbial fuel cell performance, Water Res. 45 (2011) 1571–1578, https://doi.org/10.1016/j.watres.2010.11.033.

[3] L. Woodward, M. Perrier, B. Srinivasan, R.P. Pinto, Tartakovsky, comparison of real-time methods for maximizing power output in microbial fuel cells, AIChE J. 56 (2010) 2742–2750, https://doi.org/10.1002/aic.12157.

[4] D. Molognoni, S. Puig, M.D. Balaguer, A.G. Capodaglio, A. Callegari, J. Colprim, Multiparametric control for enhanced biofilm selection in microbial fuel cells, J. Chem. Technol. Biotechnol. 91 (2016) 1720–1727, https://doi.org/10.1002/jctb.4760.

[5] J.-D. Park, Z. Ren, Hysteresis controller based maximum power point tracking energy harvesting system for microbial fuel cells, J. Power Sources 205 (2012) 151–156, https://doi.org/10.1016/j.jpowsour.2012.01.053.

[6] M. Alaraj, M. Radenkovic, J.-D. Park, Intelligent energy harvesting scheme for microbial fuel cells: maximum power point tracking and voltage overshoot avoidance, J. Power Sources 342 (2017), https://doi.org/10.1016/j.jpowsour.2016.12.104.

[7] A. Meehan, H. Gao, Z. Lewandowski, Energy harvesting with microbial fuel cell and power management system, IEEE Trans. Power Electron. 26 (2011) 176–181, https://doi.org/10.1109/TPEL.2010.2054114.

[8] U. Karra, E. Muto, R. Umaz, M. Kölln, C. Santoro, L. Wang, B. Li, Performance evaluation of activated carbon-based electrodes with novel power management system for long-term benthic microbial fuel cells, Int. J. Hydrog. Energy 39 (2014) 21847–21856, https://doi.org/10.1016/j.ijhydene.2014.06.095.

[9] N. Tang, W. Hong, T. Ewing, H. Beyenal, J. Kim, A Self-Sustainable Power Management System for Reliable Power Scaling Up of Sediment Microbial Fuel Cells 30 (2015) 4626–4632, https://doi.org/10.1109/TPEL.2015.2397931.

[10] E. Dallago, A.L. Barnabei, A. Liberale, G. Torelli, G. Venchi, A 300-mV low-power management system for energy harvesting applications, IEEE Trans. Power Electron. 31 (2016) 2273–2281, https://doi.org/10.1109/TPEL.2015.2431439.

[11] S. Carreon-Bautista, C. Erbay, A. Han, E. Sánchez-Sinencio, Power management system with integrated maximum power extraction algorithm for microbial fuel cells, IEEE Trans. Energy Convers. 15 (2015) 262, https://doi.org/10.1109/JSSC.2014.2354645.

[12] H.C. Boghani, R.M. Dinsdale, A.J. Guwy, G.C. Premier, Sampled-time control of a microbial fuel cell stack, J. Power Sources (2017), https://doi.org/10.1016/j.jpowsour.2017.03.118.

[13] H. Liu, B.E. Logan, Electricity generation using an air-cathode single chamber microbial fuel cell in the presence and absence of a proton exchange membrane, Environ. Sci. Technol. 38 (2004) 4040–4046, https://doi.org/10.1021/Es0499344.

[14] Z. Du, H. Li, T. Gu, A state of the art review on microbial fuel cells: a promising technology for wastewater treatment and bioenergy, Biotechnol. Adv. 25 (2007) 464–482, https://doi.org/10.1016/j.biotechadv.2007.05.004.

[15] F. Yang, K.-C. Wang, Y. Huang, Energy-neutral communication protocol for very low power microbial fuel cell based wireless sensor network, IEEE Sens. J. 15 (2015) 2306–2315, https://doi.org/10.1109/JSEN.2014.2377031.

[16] I. Lee, G. Kim, S. Bang, A. Wolfe, R. Bell, S. Jeong, Y. Kim, J. Kagan, M. Arias-Thode, B. Chadwick, D. Sylvester, D. Blaauw, Y. Lee, System-on-mud: ultra-low power oceanic sensing platform powered by small-scale benthic microbial fuel cells, IEEE Trans. Circuits Syst. I Regul. Pap. 62 (2015) 1126–1135, https://doi.org/10.1109/TCSI.2015.2390559.

[17] C. Donovan, A. Dewan, H. Peng, D. Heo, H. Beyenal, Power management system for a 2.5 W remote sensor powered by a sediment microbial fuel cell, J. Power Sources 196 (2011) 1171–1177, https://doi.org/10.1016/j.jpowsour.2010.08.099.

[18] J.-D. Park, T.M. Roane, Z.J. Ren, M. Alaraj, Dynamic modeling of a microbial fuel cell considering anodic electron flow and electrical charge storage, Appl. Energy 193 (2017), https://doi.org/10.1016/j.apenergy.2017.02.055.

[19] T. Instruments, Single Supply, MicroPower INSTRUMENTATION AMPLIFIER, Ina 122 Datasheet, (1997).

[20] N. Degrenne, F. Buret, B. Allard, P. Bevilacqua, Electrical energy generation from a large number of microbial fuel cells operating at maximum power point electrical load, J. Power Sources 205 (2012) 188–193, https://doi.org/10.1016/j.jpowsour.2012.01.082.

[21] T. Instruments, MIXED SIGNAL MICROCONTROLLER, MSP430L092 Datasheet, (2010).

[22] R. Umaz, C. Garrett, F. Qian, B. Li, L. Wang, S. Member, A Power Management System for Multianode Benthic Microbial Fuel Cells 32 (2017), pp. 3562–3570.

[23] X. Zhang, H. Ren, S. Pyo, J.-I. Lee, J. Kim, J. Chae, A high-efficiency DC-DC boost converter for a miniaturized microbial fuel cell, IEEE Trans. Power Electron. 30 (2015) 2041–2049, https://doi.org/10.1109/TPEL.2014.2323075.

[24] Y. Shih, B.P. Otis, An inductorless DC – DC converter for energy harvesting with a 1.2-μW bandgap-referenced output, Controller 58 (2011) 832–836.